Origin of electronic and optical trends in ternary $In_2O_3(ZnO)_n$ transparent conducting oxides ($n=1,3,5$): Hybrid density functional theory calculations

Aron Walsh, Juarez L. F. Da Silva, Yanfa Yan, M. M. Al-Jassim, and Su-Huai Wei
National Renewable Energy Laboratory, Golden, Colorado 80401, USA
(Received 20 October 2008; revised manuscript received 12 January 2009; published 26 February 2009)

Ternary oxides formed from zinc and indium have demonstrated potential for commercial optoelectronic applications. We present state-of-the-art hybrid density functional theory calculations for Zn-poor and Zn-rich compositions of the crystalline $In_2O_3(ZnO)_n$ compounds. We reveal the origin of the redshift in optical transitions compared to the two component oxides: symmetry forbidden band-edge transitions in In_2O_3 are overcome on formation of the superlattices, with Zn-O contributions to the top of the valence band. Increasing n results in the localization of the conduction-band minimum on the In-O networks. This enhanced localization explains why Zn-poor compounds (lower n) exhibit optimal conductivity.

DOI: 10.1103/PhysRevB.79.073105 PACS number(s): 71.20.−b, 78.20.−e, 71.15.Mb

Transparent conducting oxides (TCOs) are ubiquitous components in optoelectronic devices.[1,2] While Sn-doped In_2O_3 (ITO) is the prototype n-type TCO,[2–6] the high cost of indium is directing the search toward materials with reduced indium content. This, and the possibility of discovering new material compositions with superior properties, has led to the investigation of ternary and quaternary systems, with $In_2O_3(ZnO)_n$ (IZO) being a particular focus of attention.[7–12] These studies have highlighted the improved chemical and thermal stabilities of IZO compared to ITO, making it more desirable for commercial applications.

Zinc adopts fourfold coordination in the ZnO wurtzite structure, while indium is sixfold coordinated in the In_2O_3 bixbyite structure. As these coordination preferences are largely maintained in the crystalline $In_2O_3(ZnO)_n$ and related compounds,[13–16] similar electronic behavior would be expected for the ternary oxides; however, this is not the case. IZO compounds can exhibit improved chemical behavior, coupled with unusual optoelectronic properties, for instance, the reduction of the IZO optical band gaps much below that of ZnO (3.44 eV) (Ref. 17) and In_2O_3 (3.75 eV),[3] i.e., in the range 2.9–3.1 eV for $n=2-5$, is unexpected.[7,9]

In this Brief Report, through systematic electronic structure analysis of both Zn-rich and Zn-poor $In_2O_3(ZnO)_n$ compounds ($n=1,3,5$), we explain a number of phenomena: (i) the reduced IZO optical band gaps arise from the symmetry forbidden band-edge transitions in In_2O_3, which are overcome in IZO, where the ZnO layers contribute to the valence band (VB) edge; (ii) for higher values of n, the lowest conduction band (CB) state becomes more localized on the InO_2 octahedron layers, i.e., n-type conductivity becomes anisotropic and difficult for Zn-rich IZO; (iii) the band gaps and onset of optical absorption increase with increasing n.

Calculations were performed using density functional theory (DFT) as implemented in VASP.[18,19] The In and Zn d^{10} states were treated as valences within the projector augmented wave method and a plane-wave basis set (400 eV cutoff). Exchange and correlation effects were treated by a hybrid Heyd-Scuseria-Ernzerhof (HSE) approach,[20] in which a percentage of exact nonlocal Fock exchange (α) is added to the generalized gradient Perdew-Burke-Ernzerhof (PBE) functional[21] and a screening of $\omega=0.11$ bohr^{-1} is applied to partition the Coulomb potential into short-range (SR) and long-range (LR) terms. The exchange-correlation functional becomes

$$E_{\mathrm{xc}}^{\mathrm{HSE}}(\omega) = E_x^{\mathrm{HSE,SR}} + E_x^{\mathrm{PBE,LR}} + E_c^{\mathrm{PBE}}, \quad (1)$$

where

$$E_x^{\mathrm{HSE,SR}} = \alpha E_x^{\mathrm{Fock,SR}} + (1-\alpha)E_x^{\mathrm{PBE,SR}}. \quad (2)$$

Details of the HSE implementation in VASP are available elsewhere.[22] At this level, the calculated band gaps for ZnO and In_2O_3 are 3.39 and 2.74 eV, respectively.[23] The layered In-modulated IZO structures employed ($R\bar{3}m$ derived symmetry) were taken from recent DFT calculations,[13] which are consistent with both x-ray diffraction[14] and transmission electron microscopy[15] measurements. There are 4, 6, and 10 f.u. for the $n=1$, 3, and 5 structures, respectively (Fig. 1). A k-point grid density of $4\times4\times2$ was used for $n=1$, with similar quality meshes for higher n.

The calculated local electronic density of states (DOS) of $In_2O_3(ZnO)$ is shown in Fig. 2. The distribution of states is similar to that expected from a combination of ZnO and In_2O_3, i.e., there is a Zn d band at the bottom of the upper VB that hybridizes with O p located at the top of the VB. As the In $4d$ states lie to higher binding energy (−13.5 eV) than

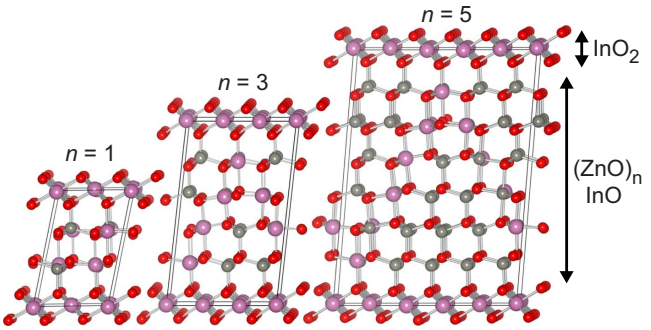

FIG. 1. (Color online) Crystallographic unit cells for $In_2O_3(ZnO)_n$, $n=1$, 3, and 5, structures (Ref. 13) viewed along [010] with pink/light gray In (large), gray zinc (medium), and red/dark gray oxygen (small). Visualization was performed with VESTA (Ref. 24).

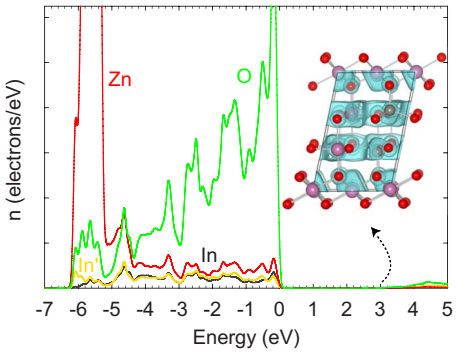

FIG. 2. (Color online) Local electronic density of states of $In_2O_3(ZnO)$, with an isosurface of the conduction-band minimum state plotted at 1 $me/Å^3$ (inset). "In" refers to In atoms in the InO_2 octahedron, while "In′" refers to In atoms in the mixed In/Zn layers.

Zn $3d$ (−5.5 eV), they make a weaker contribution to the valence states (via reduced p-d coupling). The distribution of In states from the InO_2 octahedra and mixed In/Zn layers is similar, except for hybridization of the mixed ions with Zn at −6 eV. The lower CB contains contributions from In, Zn, and O s; the delocalized nature of the CB minimum state for $n=1$ can be observed from the isosurface plot in Fig. 2. For higher values of n, the DOS features remain unchanged, except for the increased contribution of the ZnO framework to the VB and In to the CB. Assignment of the partial atomic charges from Bader analysis[25] confirms that changes on formation of the ternary systems are small (± 0.05 e/at.) in comparison to the binary parent compounds. The predicted Γ-point HSE band gaps are 2.91, 3.04, and 3.05 eV for $n=1$, 3 and 5, respectively. These offer substantial improvement over PBE alone (2.0–2.3 eV lower) and reproduce the monotonic increase empirically observed with higher n.

Recent studies have shown that the fundamental electronic band gap of In_2O_3 (~2.7 eV) is 0.8 eV less than the intrinsic optical gap due to parity forbidden optical transitions involving the band-edge states.[5,26] Decomposition of the band-edge states in IZO reveals that the VB maximum arises from the Zn-O networks, i.e., from Zn $3d$-O $2p$ hybridization, while the CB minimum is a hybridized mixture of In, Zn, and O s states (Fig. 2). It is therefore not surprising that transitions from the VB to CB extrema result in allowed optical matrix elements (>0.7 a.u.) for all values of n. This

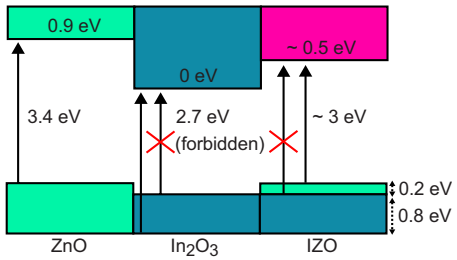

FIG. 3. (Color online) Schematic band offsets inferred from HSE calculations of the IZO superlattices. Note the fundamental optical transition is symmetry forbidden for In_2O_3 (Refs. 5 and 26) but not for IZO.

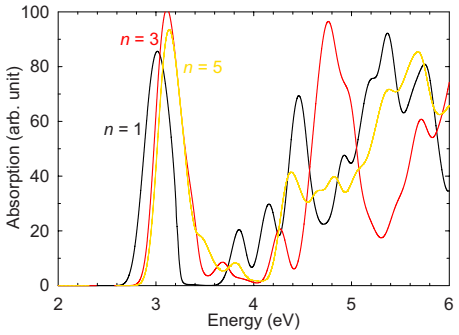

FIG. 4. (Color online) Calculated optical-absorption spectra, averaged over each symmetry component, for direct transitions in $In_2O_3(ZnO)_n$.

explains the anomaly of why the apparent optical gap of In_2O_3 (3.75 eV) (Ref. 3) is seen to reduce below 3.44 eV on the addition of ZnO to form IZO: the band-edge states from the ZnO layers now contribute to strong optical absorption. The representative valence and conduction band offsets between ZnO, In_2O_3, and IZO are shown in Fig. 3. These reproduce the recent alignment of the ultraviolet and inverse photoemission spectra from both binary oxides.[27]

Due to their rhombohedral lattices, the optical properties of the crystalline IZO systems are highly anisotropic. This is most apparent for $n=1$, where the lowest energy band-edge transitions are allowed in the z direction, but zero in the x and y planes. This dichroism results in a 100 meV blueshift in the absorption of light polarized along x and y. For higher values of n, this effect is diminished due to the higher density of bands at the top of the VB resulting from the larger superlattices (Fig. 5).

The optical-absorption spectra are shown in Fig. 4. These are summed over direct VB to CB transitions and therefore exclude indirect and intraband absorptions.[28] Excitonic effects are not treated within the framework of single-particle transitions and would require the treatment of higher order electronic structure methods.[29,30] A small blueshift is seen on transition from $n=1$ to 5, consistent with the calculated band gaps and the empirical trend. Similar absorption features are observed in each case: a strong peak centered around 3 eV, which dips and begins to rise again around 4.5 eV. The ob-

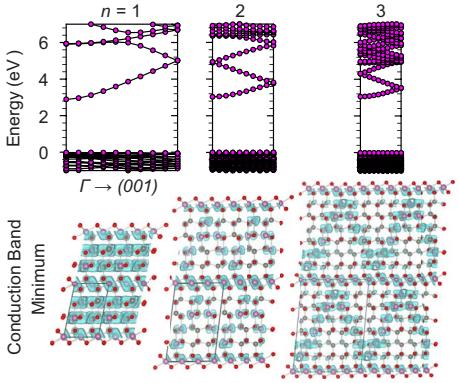

FIG. 5. (Color online) $In_2O_3(ZnO)_n$ band dispersions along $\Gamma(0,0,0)\rightarrow(0,0,\frac{1}{2})$, with isosurfaces of the corresponding conduction-band minimum state plotted at 1 $me/Å^3$ (inset).

served dip in optical absorption originates from a range of symmetry forbidden transitions below the top of the VB. The optical properties of IZO are therefore strongly influenced by those of In_2O_3 itself where dipole forbidden transitions are present,[5,31] although here band-edge VB→CB transitions are allowed due to the presence of low binding-energy ZnO states (Fig. 3).

The calculated band structures can be used to interpret the electronic behavior of the IZO compounds (Fig. 5). The top of the VB exhibits no significant dispersion, indicating a large barrier for hole mobility. In contrast, the CB are highly dispersed. For larger values of n, the effects of band folding can be observed. The spatial distribution of the CB states is critical in determining the n-type mobility and subsequent conductivity. Isosurfaces of the CB minimum states are also shown in Fig. 5. For $n=1$, only two mixed cation layers are present between the In octahedra, and these contain equal contributions from In and Zn, which results in an electron distribution spread over the entire cell (similar to a homogeneous alloy). For $n=3$ and 5, the number of intermixed layers increases to 4 and 6, respectively, and with the increased Zn concentration, a more effective superlattice is formed. Here, the carriers become more confined in the InO_2 octahedron networks; however, the modulated In ions in the ZnO layers make a significant additional contribution to the CB in $n=3$ and 5, as observed from the modulated electron-density distribution in Fig. 5. Overall, the inhomogeneity of the CB states for larger n diminishes the isotropy of the conduction network, which will in turn result in greater barriers to n-type conductivity. This correlates with the minimum in resistivity reported for IZO samples with low Zn concentrations, i.e., $0<n<1$.[7,8,12]

In summary, we have presented electronic structure and optical analysis of the crystalline $In_2O_3(ZnO)_n$ compounds with $n=1$, 3, and 5. For each composition, the VB and CB extrema are dominated by the Zn-O and In-O layers, respectively. Our results explain the origin of the redshift in optical transitions compared to the two component oxides: symmetry forbidden band-edge transitions in In_2O_3 are overcome on formation of the superlattices with the addition of ZnO. Furthermore, we observe that carrier localization on the InO_2 octahedron increases with Zn concentration, explaining why Zn-poor compounds exhibit optimal conductivity.

We thank G. Kresse for the provision of VASP 5.1 for the HSE calculations. This work is supported by the U.S. Department of Energy (DOE) under Contract No. DE-AC36-08GO28308.

[1] G. Thomas, Nature (London) **389**, 907 (1997).
[2] P. P. Edwards, A. Porch, M. O. Jones, D. V. Morgan, and R. M. Perks, Dalton Trans. **15**, 2295 (2004).
[3] I. Hamberg, C. G. Granqvist, K. F. Berggren, B. E. Sernelius, and L. Engstrom, Phys. Rev. B **30**, 3240 (1984).
[4] P. D. C. King, T. D. Veal, D. J. Payne, A. Bourlange, R. G. Egdell, and C. F. McConville, Phys. Rev. Lett. **101**, 116808 (2008).
[5] A. Walsh, J. L. F. Da Silva, S.-H. Wei, C. Körber, A. Klein, L. F. J. Piper, A. DeMasi, K. E. Smith, G. Panaccione, P. Torelli, D. J. Payne, A. Bourlange, and R. G. Egdell, Phys. Rev. Lett. **100**, 167402 (2008).
[6] A. Walsh, J. L. F. Da Silva, and S.-H. Wei, Phys. Rev. B **78**, 075211 (2008).
[7] T. Minami, H. Sonohara, T. Kakumu, and S. Takata, Jpn. J. Appl. Phys., Part 2 **34**, L971 (1995).
[8] M. P. Taylor, D. W. Readey, C. W. Teplin, M. F. A. M. van Hest, J. L. Alleman, M. S. Dabney, L. M. Gedvilas, B. M. Keyes, B. To, J. D. Perkins, and D. S. Ginley, Meas. Sci. Technol. **16**, 90 (2005).
[9] H. Hiramatsu, W.-S. Seo, and K. Koumoto, Chem. Mater. **10**, 3033 (1998).
[10] B. Kumar, H. Gong, and R. Akkipeddi, J. Appl. Phys. **98**, 073703 (2005).
[11] A. J. Leenheer, J. D. Perkins, M. F. A. M. van Hest, J. J. Berry, R. P. O'Hayre, and D. S. Ginley, Phys. Rev. B **77**, 115215 (2008).
[12] T. Moriga, T. Okamoto, K. Hiruta, A. Fujiwara, and I. Nakabayashi, J. Solid State Chem. **155**, 312 (2000).
[13] J. L. F. Da Silva, Y. Yan, and S.-H. Wei, Phys. Rev. Lett. **100**, 255501 (2008).
[14] N. Kimizuka and E. Takayama, J. Solid State Chem. **40**, 109 (1981).
[15] C. Li, Y. Bando, M. Nakamura, M. Onoda, and N. Kimizuka, J. Solid State Chem. **139**, 347 (1998).
[16] W.-J. Lee, E.-A. Choi, J. Bang, B. Ryu, and K. J. Chang, Appl. Phys. Lett. **93**, 111901 (2008).
[17] O. M. Madelung, *Semiconductors: Data Handbook*, 3rd ed. (Springer, Berlin, 2004).
[18] G. Kresse and J. Furthmüller, Phys. Rev. B **54**, 11169 (1996).
[19] G. Kresse and J. Furthmüller, Comput. Mater. Sci. **6**, 15 (1996).
[20] J. Heyd, G. E. Scuseria, and M. Ernzerhof, J. Chem. Phys. **118**, 8207 (2003).
[21] J. P. Perdew, K. Burke, and M. Ernzerhof, Phys. Rev. Lett. **77**, 3865 (1996).
[22] J. Paier, M. Marsman, K. Hummer, G. Kresse, I. C. Gerber, and J. G. Angyan, J. Chem. Phys. **124**, 154709 (2006).
[23] Due to the system-dependent screened HSE exchange required to reproduce the binary band gaps (ZnO: 37.5%; In_2O_3: 25%), the ternary electronic properties were calculated using exchange determined from $(\alpha_{In_2O_3}+n\alpha_{ZnO})/(n+1)$.
[24] K. Momma and F. Izumi, J. Appl. Crystallogr. **41**, 653 (2008).
[25] E. Sanville, S. D. Kenny, R. Smith, and G. Henkelman, J. Comput. Chem. **28**, 899 (2007).
[26] A. Bourlange, D. J. Payne, R. G. Egdell, J. S. Foord, P. P. Edwards, M. O. Jones, A. Schertel, P. J. Dobson, and J. L. Hutchison, Appl. Phys. Lett. **92**, 092117 (2008).
[27] T. Kamiya and M. Kawasaki, MRS Bull. **33**, 1061 (2008).
[28] B. Adolph, J. Furthmüller, and F. Bechstedt, Phys. Rev. B **63**, 125108 (2001).
[29] J. Paier, M. Marsman, and G. Kresse, Phys. Rev. B **78**, 121201(R) (2008).
[30] L. E. Ramos, J. Paier, G. Kresse, and F. Bechstedt, Phys. Rev. B **78**, 195423 (2008).
[31] F. Fuchs and F. Bechstedt, Phys. Rev. B **77**, 155107 (2008).